

Reentrant delocalization transition in one-dimensional photonic quasicrystals

Sachin Vaidya^{1,*}, Christina Jörg^{1,*}, Kyle Linn¹, Megan Goh², and Mikael C. Rechtsman¹

¹Department of Physics, The Pennsylvania State University, University Park, Pennsylvania 16802, USA

²Department of Physics, Amherst College, Amherst, Massachusetts 01002, USA



(Received 23 November 2022; accepted 25 July 2023; published 8 September 2023)

Waves propagating in certain one-dimensional quasiperiodic lattices are known to exhibit a sharp localization transition. We theoretically predict and experimentally observe that the localization of light in one-dimensional photonic quasicrystals is followed by a second delocalization transition for some states on increasing quasiperiodic modulation strength—an example of a reentrant transition. We further propose that this phenomenon can be qualitatively captured by a dimerized tight-binding model with long-range couplings. This work furthers our understanding of localization physics in complex systems and the impact of quasiperiodicity on light transport in photonic devices.

DOI: [10.1103/PhysRevResearch.5.033170](https://doi.org/10.1103/PhysRevResearch.5.033170)

I. INTRODUCTION

Anderson localization is the generic phenomenon of wave localization in randomly disordered media [1]. The presence of localized states implies the cessation of all wave transport in the thermodynamic limit and thus the Anderson model has provided deep insights into the nature of metal-to-insulator transitions for electrons in disordered solids [2] as well as for light propagating in disordered photonic structures [3,4]. Specifically in photonics, localization has been proposed and observed in photonic crystals (PhCs) and waveguide arrays, both in truly random [3,5–9] and quasicrystalline lattices [4,10–16]. In the latter case, light transport resulting from complex interference processes is much less well understood and this has often led to surprising effects such as multifractality of states [17,18], localization transitions in lower dimensions [10,19], and disorder-enhanced transport [20]. The study of such photonic structures is therefore of fundamental interest. Furthermore, localization of light can be employed for various photonic applications, such as for random nanolasing [21], the formation of photonic pseudogaps [22], the formation of high Q/V nanocavities [11,12,23,24], and for reducing the crosstalk between waveguides in fiber arrays for endoscopy and telecommunications [25].

In one and two dimensions, it can be shown that an infinitesimal amount of random disorder causes wave localization, but in three dimensions, a sharp transition occurs between extended and localized regimes at a finite value of disorder strength [26,27]. This transition can also occur in

one dimension when the random disorder of lattice potentials is replaced by quasiperiodicity. A model first proposed by Aubry and André consists of a one-dimensional lattice with quasiperiodic on-site energy modulation and nearest-neighbor couplings that exhibits such a sharp localization transition [19]. Specifically, the on-site potential for the n th site in a chain of atoms is modulated according to $E_n = E_0 + \xi \cos(2\pi\beta n)$, where E_0 is the unperturbed on-site energy, β is an irrational number, and ξ is the strength of the quasiperiodic modulation. For this simple model, the localization transition occurs for the entire spectrum at a single value of ξ due to a duality between the extended and localized regimes [19].

Extensions of the Aubry-André model with long-range couplings [28–30] and non-Hermiticity [31,32] were investigated theoretically and found to possess single-particle mobility edges and consequently intermediate regimes, where both extended and localized states coexist. Moreover, some dimerized tight-binding models [32–36] and driven Aubry-André systems [37] were recently found to exhibit a second reentrant transition of some states back to the extended regime. Simple two-component one-dimensional PhCs can be thought of as naturally dimerlike due to the patterning of their

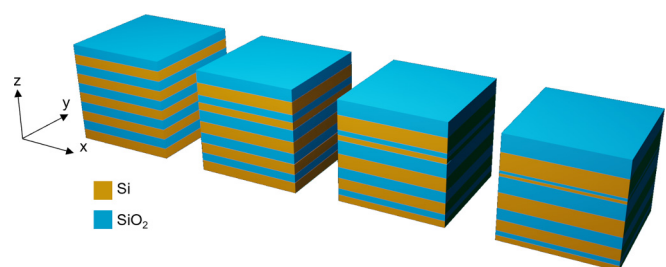


FIG. 1. Schematic of multilayer photonic structures made out of Si and SiO₂ layers. The structures have increasing quasiperiodic modulation of layer thicknesses (from left to right); the leftmost structure is a perfect one-dimensional photonic crystal and the rest are photonic quasicrystals.

*These authors contributed equally to this work.

†sachin4594@gmail.com

different dielectrics and may exhibit non-Hermiticity from gain or radiative loss. They are therefore a potentially useful platform for exploring the rich localization physics in complex quasiperiodic models.

In this paper, we experimentally demonstrate localization and delocalization phenomena in multilayer structures with quasiperiodic thickness modulation, i.e., one-dimensional photonic quasicrystals (PhQCs). We observe that in addition to the complete inhibition of transmission due to a sharp localization transition, there is a second transition to an extended regime upon increasing the quasiperiodic modulation strength. This results in the complete recovery of transmission through the structure as the quasiperiodic modulation increases well beyond the localized regime. This reentrant delocalization transition is not known to occur in random potentials and is a unique feature of quasicrystalline systems. To further explore the reentrant transition, we develop a tight-binding model inspired by our PhQCs, that captures the physics of localization and delocalization in our system.

II. NUMERICAL RESULTS AND DISCUSSION

The system considered here is shown in Fig. 1 and consists of a set of multilayer structures made out of two materials, silicon and silica (SiO_2), with refractive indices $n_{\text{Si}} = 3.5$ and $n_{\text{SiO}_2} = 1.5$, respectively. These layers are stacked along the z direction and define the dielectric function $\epsilon(z)$. When propagation purely along the z direction is considered, this system is described by the following Maxwell eigenvalue problem for a single scalar field $\mathcal{H}(z)$ [38,39],

$$-\partial_z \left(\frac{1}{\epsilon(z)} \partial_z \right) \mathcal{H}(z) = \left(\frac{\omega}{c} \right)^2 \mathcal{H}(z), \quad (1)$$

where $\mathbf{H}_{\text{TE}} = \mathcal{H}(z)\hat{\mathbf{x}}$ and $\mathbf{H}_{\text{TM}} = \mathcal{H}(z)\hat{\mathbf{y}}$ are the transverse electric (TE)- and transverse magnetic (TM)-polarized magnetic field solutions, respectively, with frequency eigenvalue ω .

Motivated by the Aubry-André model, we modulate the thicknesses of each layer in a unit cell (defined as a pair of neighboring Si and SiO_2 layers) according to

$$t_n = t_0[1 + A \cos(2\pi\beta n)], \quad (2)$$

where $n \in \{1, 2, \dots, N\}$ identifies a pair of layers, $2N$ is the total number of layers, A is the strength of the spatial modulation, and β is the closest Diophantine (rational) approximation to the golden mean, $\phi = (1 + \sqrt{5})/2$, for a given value of system size N .

When $A = 0$, all layers have the same thickness t_0 and the system is a one-dimensional (1D) PhC with a lattice constant of $a = 2t_0$, whereas for nonzero values of A , the integer sampling frequency of the cosine term and the irrational modulation frequency β provide two competing and incommensurate periods that result in a 1D PhQC. In the latter case, the average lattice constant $\langle a \rangle = 2t_0$ provides a convenient length scale. We note that since A modulates the thicknesses of layers, it is a bounded parameter with $|A| \leq 1$.

We obtain the states of our PhQCs using the plane-wave expansion method, as implemented in the open source software package MIT Photonic Bands (MPB) [40], and calculate

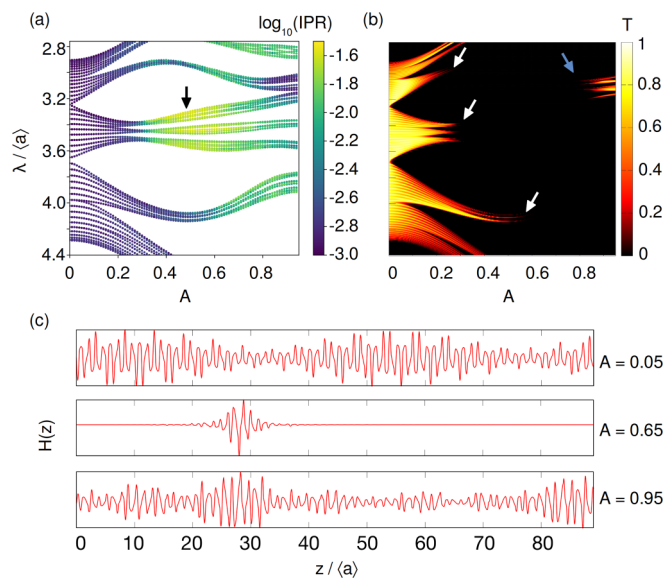


FIG. 2. (a) Eigenvalue spectrum of the PhQC states and their corresponding IPRs as a function of A for $N = 89$ and $\beta = 144/89$. (b) The transmission spectrum as a function of A for $N = 89$. Localization of various states corresponds to sharp drops in transmission (white arrows). Some states undergo a second delocalization transition around $A = 0.8$, which results in a sharp recovery of transmission (blue arrow). (c) Normalized $\mathcal{H}(z)$ -field profiles of a state near the black arrow in (a), for various values of A .

their inverse participation ratios (IPRs) given by

$$\text{IPR}_p = \frac{\int |\mathcal{H}_p(z)|^4 dz}{[\int |\mathcal{H}_p(z)|^2 dz]^2}, \quad (3)$$

where \mathcal{H}_p is the scalar field in (1), corresponding to the p th state and the integral is taken over the entire finite system. IPR is a measure of localization of states, where small (large) values of IPR indicate extended (localized) states.

The results for a system size of $N = 89$ are shown in Fig. 2. Figure 2(a) shows a plot of the eigenvalue spectrum of the PhQC states as a function of A and their corresponding IPRs. In this plot, we focus on states that constitute the second band in the PhC limit (i.e., at $A = 0$), and convert their corresponding frequency eigenvalues to dimensionless wavelength. For small values of A ($A < 0.3$), the states are extended since the structure may be thought of as being crystalline with a small quasicrystalline perturbation. For larger values of A , the states undergo transitions to a localized regime, as indicated by a sharp increase in their IPRs. However, as seen from Fig. 2(a), these transitions do not all occur at the same value of A . Moreover, for some states around $\lambda/\langle a \rangle = 3.2$ and $A = 0.8$, we observe a sharp reduction in IPRs on further increasing A , marking a reentrant transition to a second extended regime for these states. In Fig. 2(c), we also examine the $\mathcal{H}(z)$ -field profile for one such state that undergoes a reentrant transition, marked by the black arrow in Fig. 2(a). The field profiles show the transition from extended to localized and back to extended as A is increased.

Our system thus exhibits some crucial distinctions from the simple Aubry-André model. Each pair of layers that forms a unit cell in our PhQCs is not well approximated as a

resonator or atomic potential that is evanescently coupled only to its nearest neighbors. If the PhQC corresponds to a tight-binding model at all, it must be thought of as possessing long-range couplings that can be accurately computed using Wannier-function methods [41]. The presence of these effectively long-range couplings creates single-particle mobility edges that result in intermediate regimes where both extended and localized states coexist [28]. In fact, we find that due to the bounded nature of the quasiperiodic modulation strength via the parameter A , a large part of the spectrum of the PhQC remains in an intermediate regime [30]. Moreover, the states corresponding to the lowest band of the PhC limit never localize for any value of A up to its bounds (see appendices). This is because PhQCs act as effectively homogeneous dielectric media at long wavelengths. Finally, the presence of a reentrant transition suggests the breakdown of the duality between the localized and extended regimes that exists in the simple Aubry-André model.

Since the localization of states causes the cessation of wave transport, we explore its consequences in the transmission spectrum of the PhQCs. Figure 2(b) shows a plot of the transmission spectrum of the PhQCs as a function of A , calculated using a transfer-matrix approach. We see that the localization transitions from Fig. 2(a) correspond to the vanishing of transmission through the structures. This occurs because the system size here exceeds the localization length of the localized states, preventing these states from forming a transmission channel across the structures. Furthermore, we also see a recovery of transmission around $\lambda/\langle a \rangle = 3.2$, which corresponds to the reentrant transition of some of the states to an extended regime. This observation is not a finite-size effect and persists for much larger system sizes (see appendices). PhQCs and their transmission spectra therefore provide an accessible experimental setting in which to explore localization phenomena in one-dimensional systems.

III. EXPERIMENTAL RESULTS

For the experiment, we fabricate the PhQCs using plasma-enhanced chemical vapor deposition (PECVD), alternating between Si and SiO₂ deposition on a glass substrate. The deposition times control the thicknesses of each layer and are determined from (2). We fabricate a total of ten samples with $\langle a \rangle = 0.25 \mu\text{m}$, $t_0 = 0.125 \mu\text{m}$, $N = 13$, $\beta = 21/13$, and varying values of A . A scanning electron microscope (SEM) image of a typical sample is shown in Fig. 3(a). To characterize our samples, we measure the transmission spectrum of each sample as a function of wavelength, normalized to the transmission through the bare glass substrate. This is performed using a supercontinuum laser in combination with a filter that allows for wavelength selection in the range of 690–1100 nm. The transmitted power is measured with a photodiode power sensor.

The measured transmission spectrum is shown in Fig. 3(b), along with the simulation results for comparison in Fig. 3(c). We find that despite the relatively small system size, the localization transitions for states near $\lambda \sim 0.85$ and $0.75 \mu\text{m}$ are clearly observed as a sharp inhibition of transmission. Furthermore, the second transition to an extended regime near $\lambda \sim 0.78 \mu\text{m}$ is observed as a sharp recovery of transmission

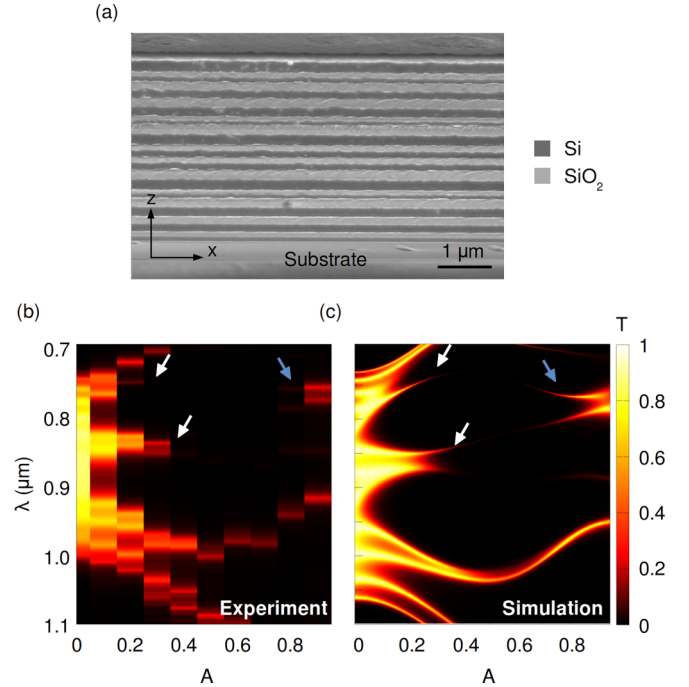


FIG. 3. (a) Scanning electron microscope (SEM) image of a cut through a typical one-dimensional photonic quasicrystal fabricated by PECVD. Both layers in a pair of neighboring Si and SiO₂ layers have identical thicknesses. The thickness values of each such pair are modulated according to Eq. (2). (b) Experimentally measured transmission spectrum as a function of A for $N = 13$. (c) Simulated transmission spectrum as a function of A for $N = 13$. In (b) and (c), the localization transitions are marked with white arrows and the reentrant delocalization transition is marked with a blue arrow.

for $A > 0.8$. The states near $\lambda \sim 1 \mu\text{m}$ are localized for $A > 0.5$, however, the system size in the experiment is smaller than the localization length of these states and as such we measure finite transmission around this wavelength (see appendices). Therefore it would be possible in principle to extract the localization length of states directly from the transmission spectrum of PhQCs by varying the system size.

IV. TIGHT-BINDING MODEL

To further explore the observed localization features, we develop a tight-binding model that qualitatively captures the physics of localization in our PhQCs. In particular, we consider a 1D quasiperiodic model with nearest- and next-nearest-neighbor couplings given by the Hamiltonian

$$\begin{aligned}
 H = & \sum_{j=A,B} \sum_{i=1}^N E_{i,j} [1 + \alpha \cos(2\pi \beta i)] n_{i,j} \\
 & - t_{NN} \sum_{i=1}^N (c_{i,A}^\dagger c_{i,B} + \text{H.c.}) - t_{NN} \sum_{i=1}^{N-1} (c_{i,B}^\dagger c_{i+1,A} + \text{H.c.}) \\
 & - t_{NNN} \sum_{j=A,B} \sum_{i=1}^{N-1} (c_{i,j}^\dagger c_{i+1,j} + \text{H.c.}), \quad (4)
 \end{aligned}$$

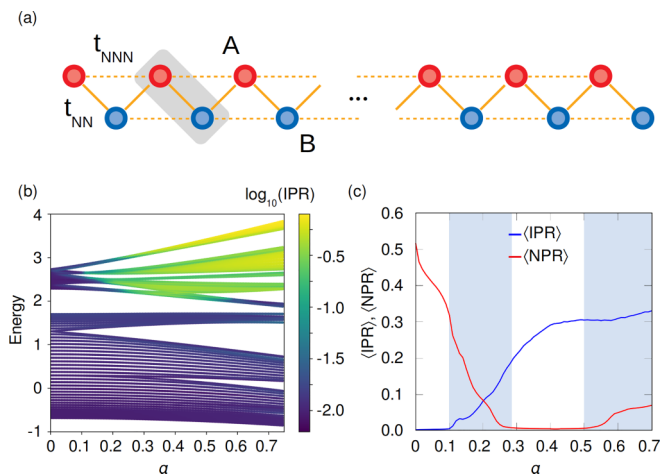


FIG. 4. (a) Schematic of the tight-binding model. The dimerized unit cell for the periodic system ($\alpha = 0$) is highlighted. The solid (dotted) lines represent nearest-neighbor (next-nearest-neighbor) couplings. (b) The energy spectrum and IPR of the states of the model for $E_{i,A} = 1$, $E_{i,B} = 2$, $t_{NN} = 0.7$, $t_{NNN} = 0.35$, and $N = 89$. The states of the second band exhibit a mobility edge and are localized for $0.25 < \alpha < 0.6$. Some states of this band undergo a reentrant delocalization transition at $\alpha \sim 0.6$. (c) A plot of the $\langle \text{IPR} \rangle$ and $\langle \text{NPR} \rangle$ for the states of the upper band for large N . The highlighted areas indicate intermediate regimes, where both $\langle \text{IPR} \rangle$ and $\langle \text{NPR} \rangle$ are nonzero, and localized and extended states coexist.

where $c_{i,j}^\dagger$, $c_{i,j}$, and $n_{i,j}$ are respectively the creation, annihilation, and number operators on site i of sublattice $j = A, B$. t_{NN} , t_{NNN} are the nearest- and next-nearest-neighbor couplings, respectively, and $E_{i,j}$ are the unperturbed on-site energies of site i of sublattice j . This lattice of $2N$ sites is shown schematically in Fig. 4(a). We choose $E_{i,A} = 1$ as the energy scale and set $\beta = (1 + \sqrt{5})/2$. α is an unbounded parameter that governs the strength of the quasiperiodic modulation of the on-site energies and we choose $E_{i,B} \neq E_{i,A}$ to introduce dimerization, akin to the two different dielectrics in the PhQCs.

We plot the IPR of the states of this model for $N = 89$ in Fig. 4(b), where we observe some important qualitative similarities with our PhQCs. The states of the lower band stay extended until a much larger value of α , compared to the upper band, similar to the lowest two bands in the PhQCs. We also observe that the states of the upper band exhibit mobility edges and an intermediate regime, before undergoing a transition to a completely localized regime at $\alpha \sim 0.25$. Moreover, some states of this band undergo a second transition at $\alpha \sim 0.6$ and remain extended for a range of α values. Eventually all states of this model become localized for a large enough value of α ($\alpha > 2$). We find that these features are generic and persist for a range of parameters of the model.

We also calculate the average IPR and average normalized participation ratio (NPR) for a set of M states, given by

$$\langle \text{IPR} \rangle = \frac{1}{M} \sum_{n=1}^M \sum_{i=1}^{2N} |\psi_{n,i}|^4, \quad (5)$$

$$\langle \text{NPR} \rangle = \frac{1}{M} \sum_{n=1}^M \left(2N \sum_{i=1}^{2N} |\psi_{n,i}|^4 \right)^{-1}, \quad (6)$$

where $|\psi_{n,i}\rangle$ is the normalized n th eigenstate of H and i labels the sites. The extended regime is characterized by near-zero $\langle \text{IPR} \rangle$ and nonzero $\langle \text{NPR} \rangle$ and vice versa for the localized regime. A nonzero value for both $\langle \text{IPR} \rangle$ and $\langle \text{NPR} \rangle$ implies the presence of an intermediate regime in the spectrum. The plot of $\langle \text{IPR} \rangle$ and $\langle \text{NPR} \rangle$ for the states of the upper band is shown in Fig. 4(c). Comparing this plot with Fig. 4(b), we can see that the first intermediate regime arises due to a mobility edge and the second intermediate regime arises due to a reentrant delocalization transition for the lowest lying states of this band.

Through this model, we see that a combination of staggered potentials and long-range couplings, competing with quasiperiodicity, can cause the delocalization of previously localized states for a range of parameter values. These findings are consistent with other models with similar qualities that are known to exhibit reentrant transitions [33–35].

V. CONCLUSION

In conclusion, we have observed a reentrant delocalization transition—a feature that is not present in the standard Aubry-André model—in 1D PhQCs with an Aubry-André-type quasiperiodic modulation. Our findings indicate, counter-intuitively, that in quasiperiodic systems, increasing the quasiperiodic modulation can fully restore light transport previously inhibited by strong localization. The PhQCs and their transmission spectra thus provide a means to experimentally explore more complex models with richer localization physics, as compared to simple nearest-neighbor tight-binding models. Inspired by the PhQCs, we have also explored the localization features of our system in a tight-binding setting in order to lend physical insight into the nature of the transitions. In the future, it will be interesting to explore localization in passive non-Hermitian 1D PhQCs enabled via a patterning of lossy dielectric materials. Furthermore, examining localized states in higher-dimensional realizations of PhQCs is warranted since it could lead to better-performing photonic nanocavities with lower-index materials.

ACKNOWLEDGMENTS

We thank Zeyu Zhang for SEM images of the PhQCs and Bill Mahoney for technical assistance with the PECVD process. C.J. acknowledges funding from the Alexander von Humboldt Foundation within the Feodor-Lynen Fellowship program. M.C.R. and S.V. acknowledge the support of the Charles E. Kaufman Foundation under Grant No. KA2020-114794, the U.S. Office of Naval Research Multidisciplinary University Research Initiative (MURI) under Grant No. N00014-20-1-2325, as well as the U.S. Army Research Office MURI under Grant No. W911NF-22-2-0103. K.L. and M.G. acknowledge support from the NSF-REU Program under Grant No. DMR-1851987.

APPENDIX A: LARGER SYSTEM SIZE AND FINITE-SIZE EFFECTS

In the main text, we mention that the reentrant transition is not a small-system-size effect but persists for much larger

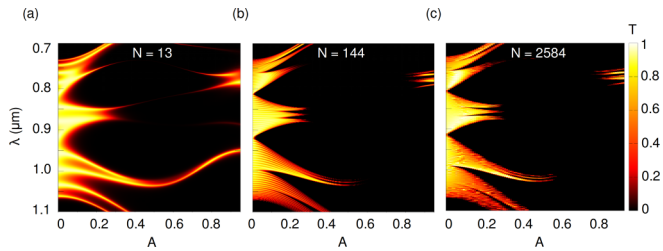


FIG. 5. (a) Transmission spectrum for $N = 13$. This is the system size fabricated in the experiment. (b) Transmission spectrum for $N = 144$. (c) Transmission spectrum for $N = 2584$. The reentrant transition occurs for arbitrarily large system sizes.

system sizes. Here, we show this using the simulated transmission spectra for a very large system size. Figures 5(a)–5(c) show the transmission spectra for a system size of $N = 13$, $N = 144$, and $N = 2584$, respectively. In all three cases, we can see the inhibition of transmission associated with the localization transitions at $\lambda \sim 0.85$ and $0.75 \mu\text{m}$, $A \sim 0.3$, and the recovery of transmission associated with the reentrant delocalization transition at $\lambda \sim 0.78 \mu\text{m}$, $A \sim 0.8$. We note that all features in the spectrum are already well converged for $N = 144$.

We next address some finite-size effects observed in our experiment. The localized regimes are characterized by modes that are exponentially localized with a characteristic localization length λ_L . If the system size is smaller than λ_L , the localized modes will be able to outcouple to vacuum due to the overlap between their evanescent tails and vacuum modes. These modes would then be detected as clear transmission channels in the spectrum. However, on increasing the system size to be larger than λ_L , these channels would no longer appear since the evanescent overlap between the modes and vacuum states would be negligible.

To further explore this, we show the simulated transmission spectra of our 1D PhQCs for various system sizes in Fig. 6 (while keeping other parameters fixed). Here, we see that the transmission channel marked with the white arrows is only present in very small system sizes ($N = 8$) and vanishes for larger sizes, including the system size considered in the experiment ($N = 13$). The corresponding state, shown in Fig. 6(h), is indeed found to be localized for $0.3 < A < 1$ with its λ_L smaller than the experimental system size. Similarly, the state marked with the blue arrows in Fig. 6 is found to be localized for $A > 0.5$ but has a larger localization length than the experimental system size and thus appears as a transmission channel in our experiments. The field profile of this state is shown in Fig. 6(g). On increasing system size to $N = 21$ and beyond, this channel also vanishes for $A > 0.5$.

APPENDIX B: INTERMEDIATE REGIMES

In the main text we state that much of the eigenvalue spectrum of the PhQCs is in an intermediate regime. In Fig. 7, we plot the spectrum for a larger frequency range along with the IPRs of the corresponding states. We notice the presence of multiple mobility edges as well as multiple reentrant delocalization transitions for various values of A . Furthermore, we also see that the lowest band does not localize for the full

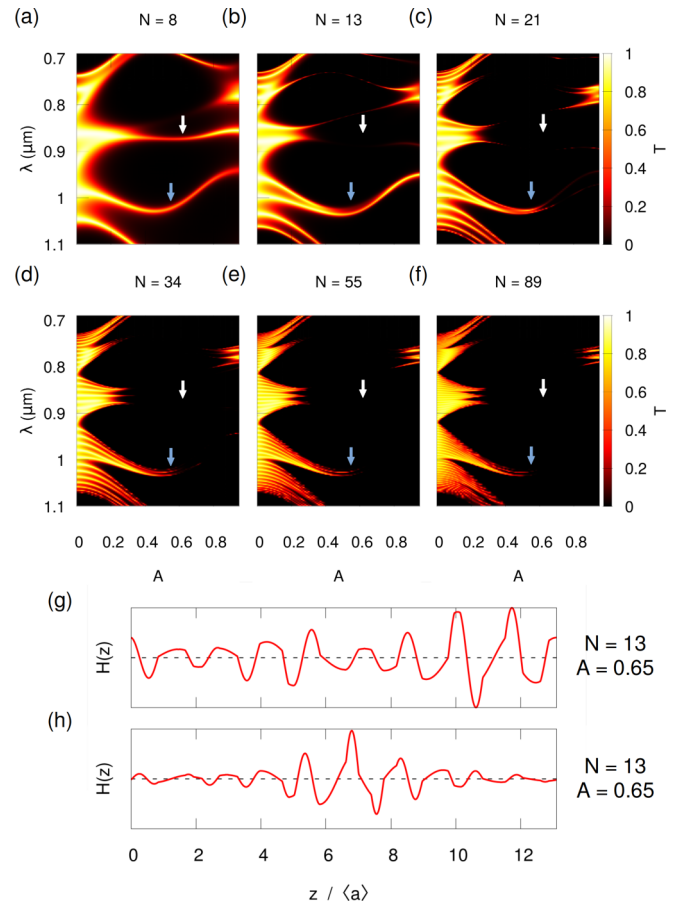


FIG. 6. Transmission spectrum vs quasiperiodic modulation strength (A) for the 1D PhQCs with varying system sizes: (a) $N = 8$, (b) $N = 13$, (c) $N = 21$, (d) $N = 34$, (e) $N = 55$, and (f) $N = 89$. (g), (h) The $\mathcal{H}(z)$ -field profiles of the states for $N = 13$ marked with the blue and white arrows, respectively.

range of A due to the behavior of these PhQCs as effectively homogeneous dielectrics at long wavelengths.

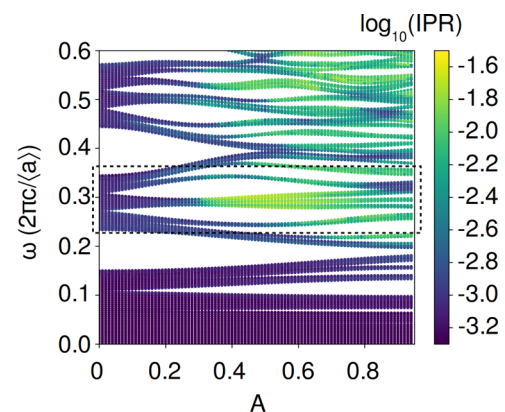


FIG. 7. The eigenvalue spectrum for the family of PhQCs considered in the main text for a larger frequency range. In the main text and in the experiment, we focus on the localization features of states in the dimensionless frequency range of 0.227 – 0.357 (dashed box) that constitute the second band of the PhC limit (i.e., at $A = 0$).

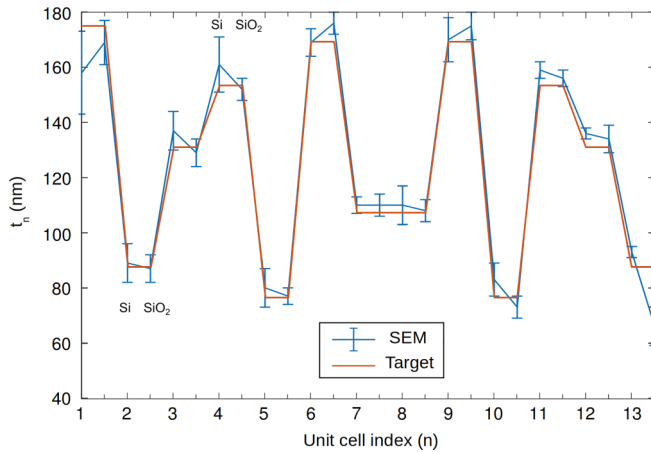


FIG. 8. Comparison of a sample's layer thicknesses extracted from SEM images (blue) and targeted thickness (red).

APPENDIX C: METHODS

For the fabrication of 1D PhQCs, we employ the plasma-enhanced chemical vapor deposition (PECVD) process to deposit alternating layers of silicon (Si) and silica (SiO_2). The layers are deposited onto a glass substrate (Corning 18-mm-square microscope glass cover slide). Si is deposited from Ar

and SiH_4 precursor gases at 220°C and a pressure of 4.5 Torr, while silica is deposited from N_2O and SiH_4 precursor gases at 300°C and pressure of 3.5 Torr. The thicknesses of the layers are controlled by the deposition time.

To characterize the fabrication imperfections in our system and show that the observed features are robust against fabrication disorder, we extract the layer thicknesses of one of the samples from SEM images and compare them with the targeted thicknesses given by Eq. (2) in Fig. 8. We observe random fluctuations in the layer thicknesses with respect to the targeted thickness by a maximum of $\pm 8\%$ and an average of 2%. This is most likely caused by the fabrication process, where the chemical reaction, and thus the layer formation, is controlled purely by a timed precursor release into the chamber (a process which inherently is prone to fluctuations). We find that these fabrication errors are not large enough to cause any meaningful deviation of the observed localization features compared to simulations.

For the measurements, a collimated, unpolarized laser beam is sent through the PhQCs at normal incidence, and the transmitted power is measured via a power meter (Thorlabs S120c). To sweep through the wavelengths in the range of 690–1100 nm, a SuperK EVO white-light laser (NKT Photonics) and a SuperK Select filter box are used. The transmitted power is normalized to that from the bare glass substrate.

- [1] P. W. Anderson, Absence of diffusion in certain random lattices, *Phys. Rev.* **109**, 1492 (1958).
- [2] A. Lagendijk, B. Van Tiggelen, and D. S. Wiersma, Fifty years of Anderson localization, *Phys. Today* **62**(8), 24 (2009).
- [3] M. Segev, Y. Silberberg, and D. N. Christodoulides, Anderson localization of light, *Nat. Photonics* **7**, 197 (2013).
- [4] Z. V. Vardeny, A. Nahata, and A. Agrawal, Optics of photonic quasicrystals, *Nat. Photonics* **7**, 177 (2013).
- [5] S. John, Strong Localization of Photons in Certain Disordered Dielectric Superlattices, *Phys. Rev. Lett.* **58**, 2486 (1987).
- [6] P.-E. Wolf and G. Maret, Weak Localization and Coherent Backscattering of Photons in Disordered Media, *Phys. Rev. Lett.* **55**, 2696 (1985).
- [7] A. Genack and N. Garcia, Observation of Photon Localization in a Three-Dimensional Disordered System, *Phys. Rev. Lett.* **66**, 2064 (1991).
- [8] Y. Lahini, A. Avidan, F. Pozzi, M. Sorel, R. Morandotti, D. N. Christodoulides, and Y. Silberberg, Anderson Localization and Nonlinearity in One-Dimensional Disordered Photonic Lattices, *Phys. Rev. Lett.* **100**, 013906 (2008).
- [9] P. García, S. Smolka, S. Stobbe, and P. Lodahl, Density of states controls anderson localization in disordered photonic crystal waveguides, *Phys. Rev. B* **82**, 165103 (2010).
- [10] Y. Lahini, R. Pugatch, F. Pozzi, M. Sorel, R. Morandotti, N. Davidson, and Y. Silberberg, Observation of a Localization Transition in Quasiperiodic Photonic Lattices, *Phys. Rev. Lett.* **103**, 013901 (2009).
- [11] F. Alpeggiani, L. C. Andreani, and D. Gerace, Effective bichromatic potential for ultra-high Q -factor photonic crystal slab cavities, *Appl. Phys. Lett.* **107**, 261110 (2015).
- [12] A. Simbula *et al.*, Realization of high- Q/V photonic crystal cavities defined by an effective Aubry-André-Harper bichromatic potential, *APL Photonics* **2**, 056102 (2017).
- [13] E. Macia, Exploiting aperiodic designs in nanophotonic devices, *Rep. Prog. Phys.* **75**, 036502 (2012).
- [14] A. D. Snel'nik *et al.*, Experimental observation of intrinsic light localization in photonic icosahedral quasicrystals, *Adv. Opt. Mater.* **8**, 2001170 (2020).
- [15] W. Gellermann, M. Kohmoto, B. Sutherland, and P. Taylor, Localization of light waves in Fibonacci Dielectric Multilayers, *Phys. Rev. Lett.* **72**, 633 (1994).
- [16] S.-Y. Jeon, H. Kwon, and K. Hur, Intrinsic photonic wave localization in a three-dimensional icosahedral quasicrystal, *Nat. Phys.* **13**, 363 (2017).
- [17] T. Fujiwara, M. Kohmoto, and T. Tokihiro, Multifractal wave functions on a Fibonacci lattice, *Phys. Rev. B* **40**, 7413 (1989).
- [18] M. Ghulinyan, C. J. Oton, L. D. Negro, L. Pavesi, R. Sapienza, M. Colocci, and D. S. Wiersma, Light-pulse propagation in Fibonacci quasicrystals, *Phys. Rev. B* **71**, 094204 (2005).
- [19] S. Aubry and G. André, Analyticity breaking and Anderson localization in incommensurate lattices, *Ann. Isr. Phys. Soc.* **3**, 133 (1980).
- [20] L. Levi *et al.*, Disorder-enhanced transport in photonic quasicrystals, *Science* **332**, 1541 (2011).
- [21] J. Liu *et al.*, Random nanolasing in the Anderson localized regime, *Nat. Nanotechnol.* **9**, 285 (2014).
- [22] L. S. Froufe-Pérez, M. Engel, J. J. Sáenz, and F. Scheffold, Band gap formation and anderson localization in disordered photonic materials with structural correlations, *Proc. Natl. Acad. Sci. USA* **114**, 9570 (2017).
- [23] J. Vasco and S. Hughes, Exploiting long-range disorder in slow-light photonic crystal waveguides: Anderson localization and ultrahigh Q/V cavities, *ACS Photonics* **6**, 2926 (2019).

- [24] L. Sapienza *et al.*, Cavity quantum electrodynamics with Anderson-localized modes, *Science* **327**, 1352 (2010).
- [25] J. Guglielmon and M. C. Rechtsman, Inducing maximal localization with fractal waveguide arrays, *Phys. Rev. A* **99**, 063807 (2019).
- [26] D. J. Thouless, A relation between the density of states and range of localization for one dimensional random systems, *J. Phys. C: Solid State Phys.* **5**, 77 (1972).
- [27] E. Abrahams, P. Anderson, D. Licciardello, and T. Ramakrishnan, Scaling Theory of Localization: Absence of Quantum Diffusion in Two Dimensions, *Phys. Rev. Lett.* **42**, 673 (1979).
- [28] J. Biddle, D. Priour, Jr., B. Wang, and S. D. Sarma, Localization in one-dimensional lattices with non-nearest-neighbor hopping: Generalized anderson and Aubry-André models, *Phys. Rev. B* **83**, 075105 (2011).
- [29] J. Biddle and S. D. Sarma, Predicted Mobility Edges in One-Dimensional Incommensurate Optical Lattices: An Exactly Solvable Model of Anderson Localization, *Phys. Rev. Lett.* **104**, 070601 (2010).
- [30] X. Li, X. Li, and S. D. Sarma, Mobility edges in one-dimensional bichromatic incommensurate potentials, *Phys. Rev. B* **96**, 085119 (2017).
- [31] S. Longhi, Metal-insulator phase transition in a non-Hermitian Aubry-André-Harper model, *Phys. Rev. B* **100**, 125157 (2019).
- [32] W. Han and L. Zhou, Dimerization-induced mobility edges and multiple reentrant localization transitions in non-Hermitian quasicrystals, *Phys. Rev. B* **105**, 054204 (2022).
- [33] S. Roy, T. Mishra, B. Tanatar, and S. Basu, Reentrant Localization Transition in a Quasiperiodic Chain, *Phys. Rev. Lett.* **126**, 106803 (2021).
- [34] S. Roy, S. Chattopadhyay, T. Mishra, and S. Basu, Critical analysis of the reentrant localization transition in a one-dimensional dimerized quasiperiodic lattice, *Phys. Rev. B* **105**, 214203 (2022).
- [35] A. Padhan, M. K. Giri, S. Mondal, and T. Mishra, Emergence of multiple localization transitions in a one-dimensional quasiperiodic lattice, *Phys. Rev. B* **105**, L220201 (2022).
- [36] V. Goblot *et al.*, Emergence of criticality through a cascade of delocalization transitions in quasiperiodic chains, *Nat. Phys.* **16**, 832 (2020).
- [37] T. Shimasaki *et al.*, Anomalous localization and multifractality in a kicked quasicrystal, [arXiv:2203.09442](https://arxiv.org/abs/2203.09442).
- [38] J. D. Joannopoulos, S. G. Johnson, J. N. Winn, and R. D. Meade, *Photonic Crystals: Molding the Flow of Light*, 2nd ed. (Princeton University Press, Princeton, NJ, 2008), <http://ab-initio.mit.edu/book>.
- [39] K. Sakoda, *Optical Properties of Photonic Crystals*, Springer Series in Optical Sciences Vol. 80 (Springer, Berlin, 2005), 2nd ed.
- [40] S. G. Johnson and J. D. Joannopoulos, Block-iterative frequency-domain methods for Maxwell's equations in a planewave basis, *Opt. Express* **8**, 173 (2001).
- [41] V. Gupta and B. Bradlyn, Wannier-function methods for topological modes in one-dimensional photonic crystals, *Phys. Rev. A* **105**, 053521 (2022).